Reflection Removal Using Low-Rank Matrix Completion

Byeong-Ju Han Jae-Young Sim
School of Electrical Engineering
Ulsan National Institute of Science and Technology, Ulsan, Korea
{bjhan, jysim}@unist.ac.kr

Abstract

The images taken through glass often capture a target transmitted scene as well as undesired reflected scenes. In this paper, we propose a low-rank matrix completion algorithm to remove reflection artifacts automatically from multiple glass images taken at slightly different camera locations. We assume that the transmitted scenes are more dominant than the reflected scenes in typical glass images. We first warp the multiple glass images to a reference image, where the gradients are consistent in the transmission images while the gradients are varying across the reflection images. Based on this observation, we compute a gradient reliability such that the pixels belonging to the salient edges of the transmission image are assigned high reliability. Then we suppress the gradients of the reflection images and recover the gradients of the transmission images only, by solving a low-rank matrix completion problem in gradient domain. We reconstruct an original transmission image using the resulting optimal gradient map. Experimental results show that the proposed algorithm removes the reflection artifacts from glass images faithfully and outperforms the existing algorithms on typical glass images.

1. Introduction

We often capture images of a target scene through glass. For example, we take photographs of the products displayed in the show window. The captured glass image includes the target scene behind the glass as well as undesired reflected scene in front of the glass, since light passes through and is reflected on a pane of glass simultaneously. Reflection removal is the process of removing such unwanted reflection artifacts from the glass images. Most existing methods model the glass image as a linear combination of a transmission image and a reflection image and reconstruct the transmission image only while suppressing the reflection image.

Several attempts have been made to remove reflection from a single glass image by exploiting prior knowledge or assumptions on the characteristics of glass images, such as gradient sparsity [8], relative smoothness [11] or ghosting cue [15]. Levin and Weiss [8] reconstructed an optimal transmission image that minimizes a cost function designed by using a distribution model of gradient in natural images. Li and Brown [11] assumed that a reflection image is smoother and thus exhibits thinner tails of gradient distribution than a transmission image. However, this assumption may not hold when strong light is reflected on a pane of glass. Shih *et al.* [15] considered double-pane windows and employed the shifted reflection images appeared in both of the front and the back surfaces of the window. However, this method may not work on glass images where the ghosted reflection is not clearly observed.

On the other hands, multiple glass images were used for reflection removal. A set of several glass images taken from a fixed camera position were used [1, 6, 13, 14]. Polarized glass images were obtained by using different angular filters, and the angle of incidence to the glass surface is computed to estimate an optimal transmission image [6, 14]. Schechner *et al.* [13] also used multiple glass images focused on different distances for reflection removal. Agrawal *et al.* [1] used two glass images taken with and without flash, respectively, to recognize reflection artifacts. Moreover, multiple images taken from different camera positions were also used [2, 3, 7, 10, 17, 18, 20]. Li and Brown [10] warped a set of multiple glass images taken at slightly different camera locations into a reference image, and separated the gradients between the transmission image and the reflection images by analyzing the occurrence characteristics of gradients across multiple images. Xue *et al.* [20] estimated dense motion fields for both of the transmitted and reflected scenes, respectively, and recovered an optimal transmission image as well as a reflection image. Reflection removal using multiple glass images is more practical, since it achieves better performance than that of using a single glass image and it does not require strong constraints on the characteristics of glass images.

In this paper, we propose a novel reflection removal algorithm using a set of multiple glass images. We first warp input multiple glass images to a reference image to align

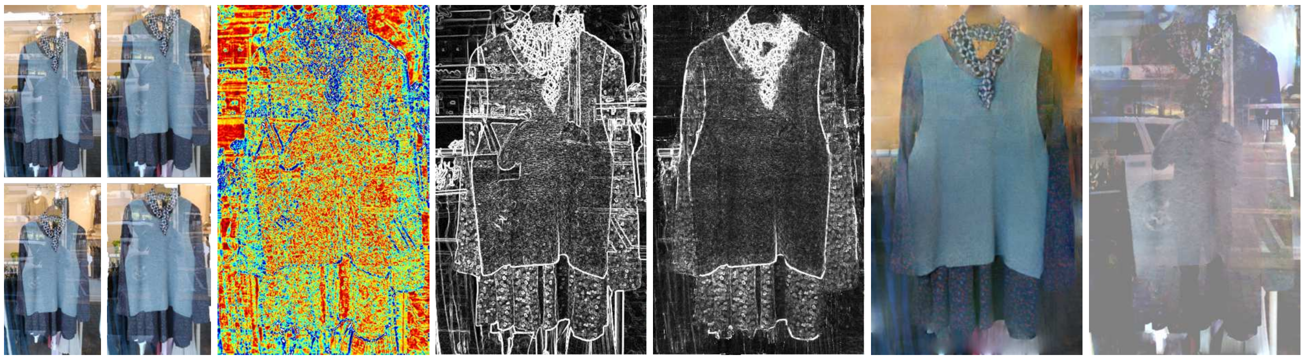

(a) (b) (c) (d) (e) (f) (g)

Figure 1. Overview of the proposed algorithm. (a) Input multiple glass images. (b) Warped glass images to a reference image. (c) Reliability map and (d) initial gradient map of the reference image. (e) Optimal gradient map for the transmission image. (f) Reconstructed transmission image. (g) Removed reflection image.

the transmission images. We compute a gradient reliability at each pixel such that a pixel with large gradient magnitude from reflection images is assigned a low reliability. We divide the gradient map of the reference image into local patches, and for a given patch, we search for the similar gradient patches from the other warped images. Then we recover the gradients of high reliability associated with the transmission image, while suppressing the gradients of low reliability coming from the reflection image by completing a given gradient patch with the similar patches based on a low-rank matrix completion framework. Finally, the resulting optimal gradient map is used to reconstruct an original color image for target transmitted scene. Note that the existing methods of reflection removal design cost functions depending on the gradient values at specified pixels selected by user assistance [8] or determined by gradient occurrence [10], and obtain transmission images by solving optimization problems based on the gradient sparsity assumption. Hence these approaches cannot sufficiently resolve the ambiguity of gradient values at undetermined pixels especially in textured regions. However, the proposed algorithm faithfully recovers the gradients of transmission image by exploiting similar gradients from the other views based on low-rank matrix completion. Experimental results show that the proposed algorithm reconstructs original transmission images from glass images faithfully while suppressing undesired reflection artifacts effectively.

The remaining of this paper is organized as follows. Section 2 explains the proposed algorithm. Section 3 shows the experimental results. Section 4 concludes the paper.

2. Proposed Algorithm

We propose a reflection removal algorithm using multiple glass images. We also model a glass image as a linear combination of a transmission image and a reflection image, such that the pixel value $I_k(\mathbf{p})$ of the k-th glass image I_k is given by

$$I_k(\mathbf{p}) = T_k(\mathbf{p}) + R_k(\mathbf{p}), \quad k = 0, 1, ..., K-1, \tag{1}$$

where T_k and R_k denote the transmission image and the reflection image in I_k, respectively, and K is the number of multiple glass images. We regard reflection removal as a problem of gradient completion for transmission image, and solve this problem by adopting low-rank matrix completion in gradient domain. Fig. 1 shows the overall process of the proposed algorithm. Input multiple glass images are first warped to a reference image. The reliability map is computed on the initial gradients in a reference glass image where the edge pixels in reflection images are assigned low reliability. Then we restore the gradients of transmission image and suppress the gradients of reflection image by using low-rank matrix completion in gradient domain. Finally, the resulting transmission gradients are used to reconstruct an original transmission image.

2.1. Multiple Image Warping

We assume that a set of multiple glass images are captured at slightly different camera locations toward a target scene behind glass. It means that the multiple glass images have similar transmission images to one another while reflection images are varying across the multiple glass images. We also assume that the transmitted scene dominates glass images compared to the reflected scenes. Therefore, when we warp the multiple glass images into a same image domain, the computed warping transform mainly depends on the features of the transmission images.

Based on this property, as did in [10], we first warp the multiple glass images to a reference image using SIFT-flow [12]. Let $\hat{I}_k$, $\hat{T}_k$ and $\hat{R}_k$ denote the warped images of I_k, T_k and R_k, respectively. Since the warping is estimated by dominant transmitted scene, $\hat{T}_k$'s are well matched to

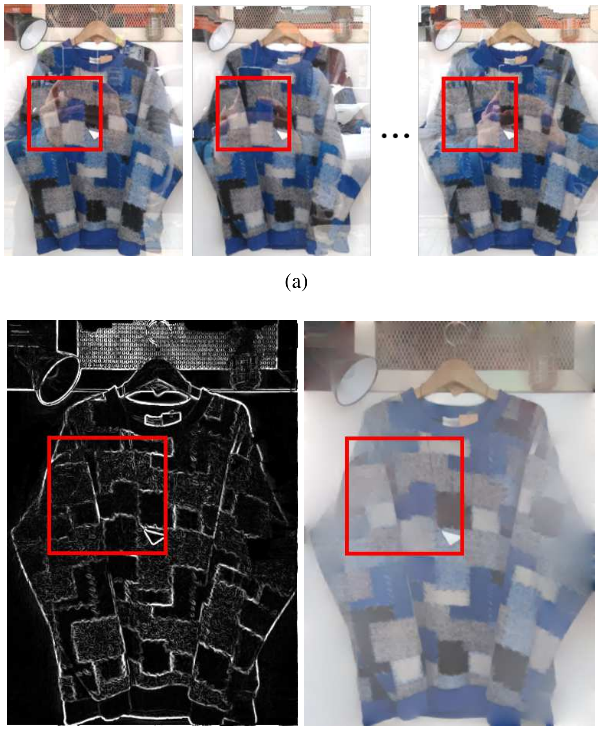

(a)

(b) (c)

Figure 2. The gradient map with the minimum magnitudes. (a) Warped glass images. (b) The gradient map with the minimum magnitudes. (c) The color image reconstructed from (b). The values of the gradient map are amplified for visualization purpose.

one another while $\hat{R}_k$'s are largely different from one another. Thus we have the following relationship:

$$\hat{I}_k(\mathbf{p}) = \hat{T}_k(\mathbf{p}) + \hat{R}_k(\mathbf{p}) \simeq T(\mathbf{p}) + \hat{R}_k(\mathbf{p}) \tag{2}$$

where T denotes the true transmitted image in the reference glass image.

2.2. Gradient Characteristics of Glass Images

We investigate the characteristics of gradients in the warped glass images. In practice, we filter the gradient maps by using the Gaussian filter with standard deviation of 1 to alleviate the effect of noisy gradients and the errors in warping transform. Also, the proposed algorithm processes the x and y directional gradient maps independently. For simpler notation, we hence use ∇ to represent either the x directional derivative or the y directional derivative.

From (2), we have

$$\nabla\hat{I}_k(\mathbf{p}) \simeq \nabla T(\mathbf{p}) + \nabla\hat{R}_k(\mathbf{p}) \tag{3}$$

which means that the gradients of transmission images are consistent while that of reflection images are varying across the warped glass images. Moreover, according to the property of sparse gradient in natural images [8], we can assume that salient edges belonging to the transmission image and the reflection image rarely appear at the same pixel locations simultaneously. In other words, at a given pixel $\mathbf{p}$ with large $|\nabla\hat{I}_k(\mathbf{p})|$, either $|\nabla T(\mathbf{p})| \gg |\nabla\hat{R}_k(\mathbf{p})|$ or $|\nabla T(\mathbf{p})| \ll |\nabla\hat{R}_k(\mathbf{p})|$ holds. Therefore, we approximate the magnitude of gradient as

$$|\nabla\hat{I}_k(\mathbf{p})| \simeq |\nabla T(\mathbf{p})| + |\nabla\hat{R}_k(\mathbf{p})|. \tag{4}$$

We observe the magnitude of gradient across multiple warped images. From (4), when $\mathbf{p}$ lies on a salient edge of the transmission image, it is highly probable that multiple warped images have a consistent large value of $|\nabla T(\mathbf{p})|$ and negligible small $|\nabla\hat{R}_k(\mathbf{p})|$'s at $\mathbf{p}$. However, when $\mathbf{p}$ lies on a salient edge of one of the reflection images, $|\nabla T(\mathbf{p})|$ becomes relatively small in all images and $|\nabla\hat{R}_k(\mathbf{p})|$'s are also small except the one image.

We define $\mathcal{G}_{\text{min}}$ as the map of gradient with the minimum magnitude among the warped glass images such that

$$\mathcal{G}_{\text{min}}(\mathbf{p}) = \underset{\nabla\hat{I}_k(\mathbf{p})}{\arg\min} \left\{ |\nabla\hat{I}_k(\mathbf{p})| \right\}. \tag{5}$$

Based on the observed characteristics of gradients in typical glass images, $\mathcal{G}_{\text{min}}$ is close to ∇T which is derived from the true transmission image.

Fig. 2 shows $\mathcal{G}_{\text{min}}$ obtained from a set of warped glass images. The red boxes indicate the photographer's hands reflected on a pane of glass. Fig. 2(a) shows that the reflected scenes are varying across the multiple images, but the transmitted scene is consistent in the multiple images. Also, as shown in the red box in Fig. 2(b), $\mathcal{G}_{\text{min}}$ rarely highlights the salient edges associated with the reflected scenes. Hence we regard $\mathcal{G}_{\text{min}}$ as an estimate of the gradient map for the desired transmission image. Fig. 2(c) shows a color image reconstructed from $\mathcal{G}_{\text{min}}$ by using [16], where we see that the undesired reflection artifacts are successfully removed, but the salient contours and textures of the transmission image are also blurred.

2.3. Gradient Reliability

To estimate the gradient map for the transmission image more reliably, we compute a reliability map Π_k for each warped glass image $\hat{I}_k$, such that the pixels having large gradient magnitudes associated with the reflection images are assigned low reliability values, and high values otherwise. In practice, we define

$$\Pi_k(\mathbf{p}) = \exp\left(-\alpha\frac{\delta(\mathbf{p})}{\sigma_\delta}\right) \tag{6}$$

where $\delta(\mathbf{p}) = |\nabla\hat{I}_k(\mathbf{p})| - |\mathcal{G}_{\text{min}}(\mathbf{p})|$, and σ_δ is the standard deviation of $\delta(\mathbf{p})$'s in $\nabla\hat{I}_k$. α is empirically set to 3.

Specifically, when $\mathbf{p}$ comes from a homogeneous region having relatively small $|\nabla\hat{I}_k(\mathbf{p})|$, then $\Pi_k(\mathbf{p})$'s have high

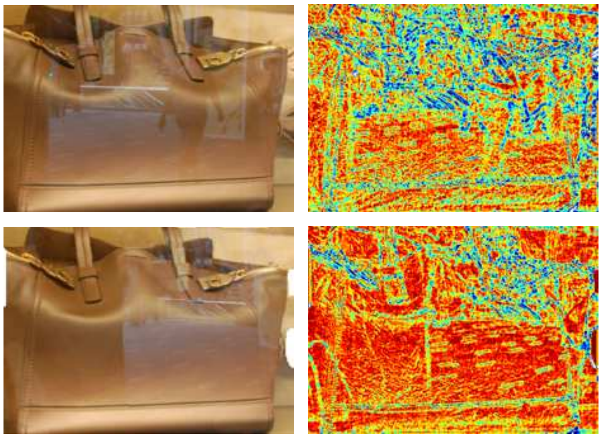

(a) (b)

Figure 3. Gradient reliability maps. (a) Two warped glass images and (b) their gradient reliability maps.

reliability values for all the multiple images since all of the $|\nabla \hat{I}_k(\mathbf{p})|$'s are similarly small. Also, when $\mathbf{p}$ lies on a salient edge of the transmission image T, $|\nabla \hat{I}_k(\mathbf{p})|$'s have almost same large values across the multiple images and thus $\Pi_k(\mathbf{p})$'s become close to 1 for all the multiple images. On the contrary, when $\mathbf{p}$ comes from a salient edge in one of the multiple reflection images, $|\nabla \hat{I}_k(\mathbf{p})|$ becomes large in only one image while $|\mathcal{G}_{\text{min}}(\mathbf{p})|$ is relatively small, which results in a low reliability of $\Pi_k(\mathbf{p})$. In this work, we compute a gradient reliability map for each color channel, respectively, and take the average reliability map for the three color channels.

Fig. 3 shows two warped glass images and their corresponding reliability maps where red and blue colors depict high and low reliability values, respectively. We observe that the homogeneous regions and the salient edges of the transmission image are assigned high reliability values, while the edges of the reflection images are assigned low values, for example the silhouette of the person in the first image and the pattern on the sidewalk in the second image. Note that, some pixels located on the salient edges of the transmission image have relatively low reliability values in one image, but the corresponding pixels in another image usually have high reliability values.

2.4. Gradient Completion for Transmission Image

We estimate the gradient map associated with only the transmission image by suppressing the gradients of low reliability derived from the reflection images. We formulate this gradient estimation as a low-rank matrix completion problem in gradient domain, called *gradient completion*. Low-rank matrix completion has been used in many applications such as image classification [21], restoration [4], saliency detection [9] and deraining [5]. However, to the best of our knowledge, this is the first attempt to apply the low-rank matrix completion technique to image gradient domain for reflection removal.

Based on the assumptions and observations on typical glass images, we see that the warped glass images exhibit a consistent and dominant gradient map of the transmission image while exhibiting varying gradient maps of the reflection images. It means that a pixel on a strong reflection edge in one image has a low reliability value, but it should have high reliability values in the other images. Therefore, we can recover optimal transmission gradients at the pixels on the reflection edges in one image by using the transmission gradients from the other images. In particular, we perform the gradient completion in a patch-wise manner. We first divide an initial gradient map of a reference glass image into local patches. Then we suppress the gradients associated with the reflection image by completing each gradient patch using the similar patches selected from the gradient maps of the other warped glass images.

Without loss of generality, let us take the first image $\hat{I}_0$ among K glass images as a reference image to be recovered. Let $\mathbf{g}$ be the column vector of a local patch of the gradient map $\nabla \hat{I}_0$. We search for $2(K-1)$ most similar patches to $\mathbf{g}$ from the other $K-1$ gradient maps $\nabla \hat{I}_k$'s for $k = 1, 2, ..., K-1$. We define a distance $d(\mathbf{g}_i, \mathbf{g}_j)$ between two gradient patches $\mathbf{g}_i$ and $\mathbf{g}_j$ as a sum of weighted squared differences between the corresponding gradient values, given by

$$d(\mathbf{g}_i, \mathbf{g}_j) = \left\| \mathbf{w}_{ij} \circ (\mathbf{g}_i - \mathbf{g}_j) \right\|_2 \tag{7}$$

where $\circ$ is the element-wise multiplication. $\mathbf{w}_{ij}$ is a weight vector associated with a pair of $\mathbf{g}_i$ and $\mathbf{g}_j$ which is computed by using the corresponding reliability values.

$$\mathbf{w}_{ij} = \frac{1}{Z_{ij}} (\boldsymbol{\pi}_i \circ \boldsymbol{\pi}_j) \tag{8}$$

where $\boldsymbol{\pi}$ is a column vector of the reliability values of gradients in the patch $\mathbf{g}$, and Z_{ij} is a normalizing factor which makes the sum of all elements in $\mathbf{w}_{ij}$ becomes 1. Note that the distance $d(\mathbf{g}_i, \mathbf{g}_j)$ compares the gradients mainly at the pixels in reflection-free areas, and less considers the edges in the reflection images, according to their reliability.

Then we construct a matrix $\mathbf{G}$ composed of the target patch $\mathbf{g}$ and the $2(K-1)$ most similar patches $\mathbf{g}_i$'s, given by

$$\mathbf{G} = \left[\mathbf{g}, \mathbf{g}_1, \mathbf{g}_2, ..., \mathbf{g}_{2(K-1)}\right]. \tag{9}$$

Note that $\hat{I}_k$'s are matched to one another by warping. Thus we find the patches $\mathbf{g}_i$'s, most similar to a target patch $\mathbf{g}$ in $\nabla \hat{I}_0$, only within the 5 pixel distance from the matched locations in the other gradient maps $\nabla \hat{I}_k$'s, respectively. We also generate a matrix $\boldsymbol{\Pi}$ using the corresponding reliability values to $\mathbf{G}$, given by

$$\boldsymbol{\Pi} = \left[\boldsymbol{\pi}, \boldsymbol{\pi}_1, \boldsymbol{\pi}_2, ..., \boldsymbol{\pi}_{2(K-1)}\right]. \tag{10}$$

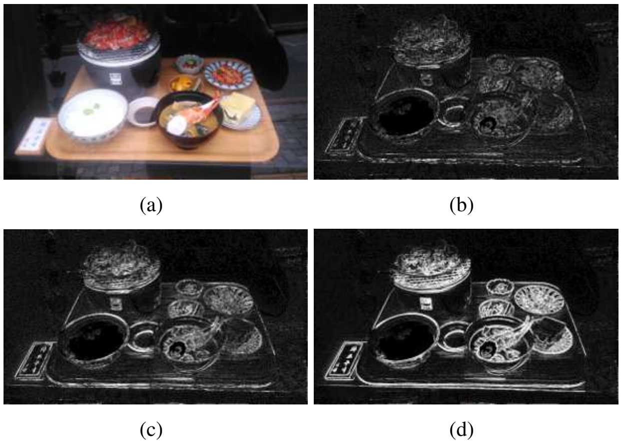

Figure 4. Gradient completion. (a) An input reference glass image. The completed gradient maps for the transmission image at the (b) 1st, (c) 2nd, and (d) 10th iterations, respectively. The values of gradient maps are amplified for visualization purpose.

Then we apply a low-rank matrix completion scheme to recover a complete gradient matrix $\mathbf{X}$ from $\mathbf{G}$, which is associated with the transmission image. We adopt the two constraints. First constraint is given by

$$\mathbf{\Pi} \circ \mathbf{X} = \mathbf{\Pi} \circ \mathbf{G} \tag{11}$$

which encourages the resulting matrix $\mathbf{X}$ preserves the original gradients in $\mathbf{G}$ at the pixels in the reflection-free areas with high reliability values. Second constraint is given by

$$|(\mathbf{1} - \mathbf{\Pi}) \circ \mathbf{X}| \leq |(\mathbf{1} - \mathbf{\Pi}) \circ \mathbf{G}| \tag{12}$$

where $\mathbf{1}$ is the matrix of all 1 elements, and $\leq$ and $|\cdot|$ denote the element-wise inequality and the element-wise absolute value operator, respectively. It means that the magnitude of the recovered gradient should be equal to or less than that of the original gradient, from (4). Consequently, we formulate a low-rank matrix completion problem as

$$\begin{aligned} \text{minimize} \quad & \|\mathbf{X}\|_* \\ \text{subject to} \quad & \mathbf{\Pi} \circ \mathbf{X} = \mathbf{\Pi} \circ \mathbf{G}, \\ & |(\mathbf{1} - \mathbf{\Pi}) \circ \mathbf{X}| \leq |(\mathbf{1} - \mathbf{\Pi}) \circ \mathbf{G}|, \end{aligned} \tag{13}$$

where $\|\mathbf{X}\|_*$ is the nuclear norm of $\mathbf{X}$.

To obtain an optimal solution to (13), we apply the expectation maximization (EM) algorithm [5, 19] in an iterative manner. An initial $\mathbf{X}^{(0)}$ is set to $\mathbf{\Pi} \circ \mathbf{G}$ to suppress the gradients with low reliability. At the t-th iteration, a low-rank estimate $\mathbf{Y}^{(t)}$ is obtained by thresholding the singular values of $\mathbf{X}^{(t)}$ with a threshold of 0.7. Then we replace the elements in $\mathbf{Y}$ not satisfying the constraint in (12) with that of $\mathbf{G}$. We update the solution matrix as $\mathbf{X}^{(t+1)} = \mathbf{\Pi} \circ \mathbf{G} + (\mathbf{1} - \mathbf{\Pi}) \circ \mathbf{Y}^{(t)}$ considering the constraint in (11). The iteration stops when $\left\|\mathbf{Y}^{(t+1)} - \mathbf{Y}^{(t)}\right\|_F < 0.01$, where $\|\cdot\|_F$ is the Frobenius norm, or when the number of iterations exceeds 10. Hence we obtain a resulting gradient map $\mathcal{G}_{\text{comp},0}$ completed from the initial gradient map of the reference image. In a same way, we can also obtain a completed gradient map $\mathcal{G}_{\text{comp},k}$ by applying the low-rank matrix completion algorithm to the k-th warped glass image.

Note that the local patches partially overlap one another by half of the patch size, and thus more than one completed gradients are computed at each pixel. We take the gradient of the largest magnitude to exploit the information of original image. Also, the gradient completion process is performed on each color channel, respectively. Fig. 4 shows the results of gradient completion on an input glass image shown in Fig. 4(a) where the photographer's body is a reflection artifact. Figs. 4(b), (c) and (d) visualize the estimated gradient maps for the transmission image at the first, second, and 10th iterations, respectively. We see that, at the first iteration, the gradients of the reflection image are successfully removed, but the gradients of the transmission image are also suppressed. However, as iteratively completing the low-rank matrix $\mathbf{X}$, the resulting gradient map highlights most of the salient edges in the transmission image faithfully as shown in Fig. 4(d).

2.5. Reconstruction of Transmission Image

Finally, we obtain an optimal gradient map $\mathcal{G}_{\text{opt}}$ for the transmission image by selecting the gradient of the largest magnitude at each pixel among the completed gradient maps $\mathcal{G}_{\text{comp},k}$'s, such that

$$\mathcal{G}_{\text{opt}}(\mathbf{p}) = \underset{\mathcal{G}_{\text{comp},k}(\mathbf{p})}{\arg\max} \left\{ |\mathcal{G}_{\text{comp},k}(\mathbf{p})| \right\}. \tag{14}$$

Then we reconstruct a color image for the transmitted scene from $\mathcal{G}_{\text{opt}}$ using [16], where we initialize the color values at the boundary pixels as the minimum colors among the multiple warped images.

3. Experimental Results

We evaluate the performance of the proposed algorithm using 32 test sets of glass images: 12 test sets are provided in [10], 2 test sets are provided in [20], and 18 test sets are newly captured. Each test set is composed of from three to seven glass images taken at slightly different camera locations. We use a patch size of 32×32 for gradient completion. In this paper, we show the reflection removal results on 12 test sets of glass images, and that of the remaining sets are provided in the supplementary material.

Fig. 5 shows the performance of the proposed reflection removal algorithm. Figs. 5(a) and (b) show the reference glass images. The initial gradient maps shown in Fig. 5(c) include the salient edges of the transmission images as well as the reflection images together, however, the resulting optimal gradient maps preserve the edges of the transmission

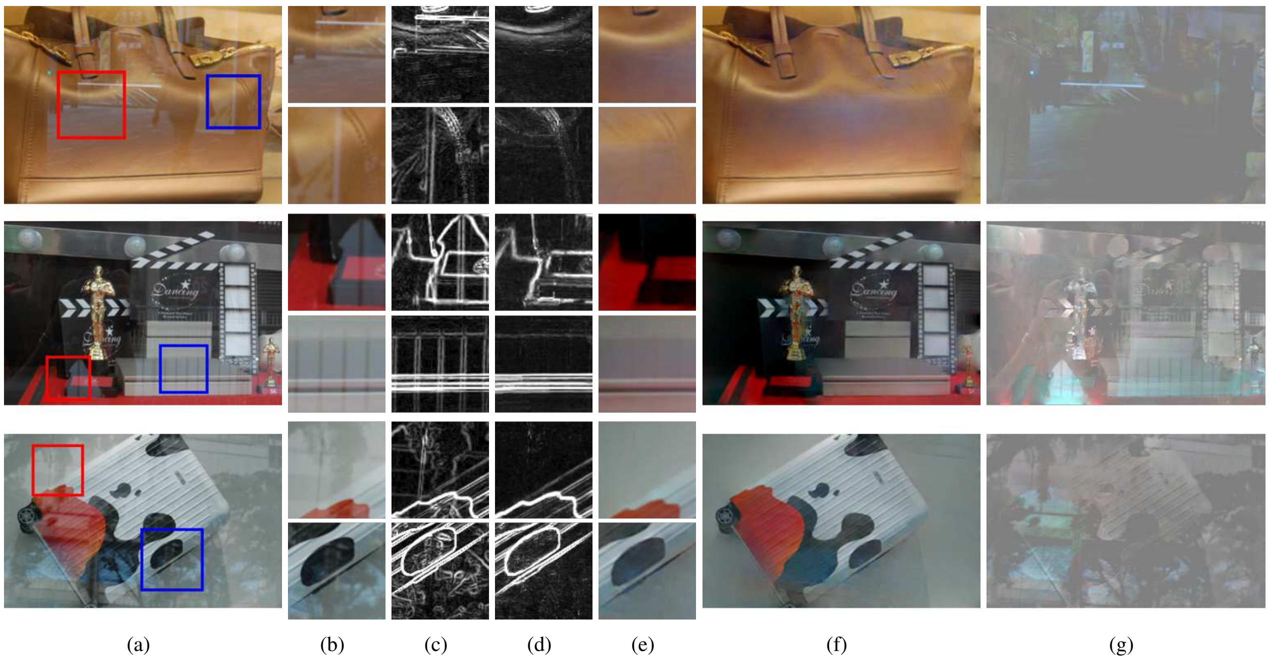

Figure 5. Reflection removal results of the proposed algorithm. (a) Reference glass images. (b) Reference glass images and (c) the initial gradient maps in zoomed-in areas. (d) The completed optimal gradient maps and (e) the reconstructed transmission images in zoomed-in areas. (f) The reconstructed transmission images and (g) the suppressed reflection images.

Figure 6. Comparison of the reflection removal algorithms. (a) Reference glass images. (b) The reconstructed transmission images by using (b) [11], (c) [10] and (d) the proposed algorithm, respectively.

images only and suppress the edges of the reflection images as shown in Fig. 5(d). Figs. 5(e) and (f) represent the reconstructed color images for the transmitted scenes, and Fig. 5(g) shows the removed reflection images. We see that the proposed algorithm faithfully reconstructs the target transmitted scenes, for example, the bag and the suitcase,

(a) (b) (c) (d)

Figure 7. More comparison of the reflection removal algorithms. (a) Reference glass images. (b) The reconstructed transmission images by using (b) [11], (c) [10] and (d) the proposed algorithm, respectively.

and effectively suppresses the unwanted reflected scenes, for example, the photographer.

We compare the results of the proposed algorithm with that of the two existing methods: [10] and [11]. We use the source codes for [10] and [11] provided in the authors' website[1]. While [10] uses multiple glass images, [11] uses a single glass image for reflection removal. Fig. 6 compares the reconstructed transmission images from the reference glass images on two test sets containing complex patterns and textures. The reflection artifacts still exist in the single image based method as shown in Fig. 6(b). As shown in Fig. 6(c), [10] yields more plausible results than that of [11]. However, it fails to preserve the original textures in the transmitted scenes accurately, since the gradients in textured regions are estimated by solving an optimization problem based on the gradient sparsity assumption. In contrary, the proposed algorithm adopts low-rank matrix completion and recovers the gradients of the transmitted scene in textured regions using the similar gradients searched from the multiple images, and therefore provides more faithful transmission images as shown in Fig. 6(d).

Fig. 7 also compares the reflection removal algorithms on more test sets of glass images, where we observe similar results. As shown in the first to third rows, [10] yields comparable results to that of the proposed algorithm. However, [10] sometimes changes the original colors of the transmitted scenes significantly and fails to correctly separate the gradients between transmission images and reflection images, as shown in the last two rows. On the contrary, the proposed algorithm provides desired transmission images reliably in most test images. However, the proposed algorithm and the existing technique [10] fail to recover the transmission image faithfully for the neck of the mannequin as shown in the third row of Fig. 7, since the SIFT-flow provides locally misaligned images. Consequently, the experimental results demonstrate that the proposed algorithm outperforms the existing methods qualitatively and is a more promising tool for reflection removal.

In addition, Fig. 8 provides the comparative results of the proposed algorithm and Xue *et al.*'s method [20]. Since the source code of [20] is not publicly available, we use the two datasets and the results of [20] which are uploaded in the authors' website[2]. Note that [20] estimates dense motion fields for not only the transmission image but the reflection image, respectively, while the proposed algorithm warps multiple glass images by using the features of transmission images mainly based on the assumption that the transmitted scenes are much more dominant than the reflected scenes in typical glass images. Both of the proposed algorithm and [20] achieve good results on the glass image in Fig. 8(a) which satisfies our assumption. However, the proposed algorithm fails to work on the glass image in Fig. 8(b), where the reflection image of the check shirt is comparably dominant to the transmission image.

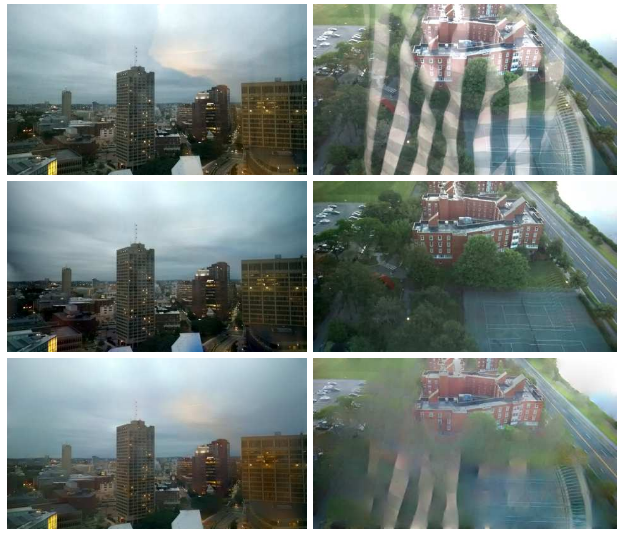

(a) (b)

Figure 8. Comparison of the reflection removal results on the two datasets in [20]. From top to bottom, reference glass images, the reconstructed transmission images by using [20] and the proposed algorithm, respectively.

4. Conclusion

In this paper, we adopted a low-rank matrix completion technique for reflection removal of multiple glass images. We first warp the multiple glass images to a reference image under the assumption that transmitted scenes exhibit more dominant features than reflected scenes in typical glass images. We design gradient reliability of pixels by using the characteristics that the warped transmission images are consistent while the warped reflection images are varying across the multiple glass images. Then we perform the low-rank matrix completion in gradient domain to recover the gradients of the transmission image while suppressing the gradients of the reflection images. The resulting optimal gradients are used to reconstruct a transmission image. Experimental results demonstrate the proposed algorithm yields a faithful result of reflection removal and outperforms the existing algorithms on typical glass images with dominant transmitted scenes. Future research includes the extension of the low-rank matrix completion concept for reflection removal using a single glass image.

Acknowledgements

This work was supported by the National Research Foundation of Korea(NRF) grant funded by the Korea government(MSIP) (No. 2017R1A2B4011970).

[1] http://yu-li.github.io

[2] https://sites.google.com/site/obstructionfreephotography

References

[1] A. Agrawal, R. Raskar, S. K. Nayar, and Y. Li. Removing photography artifacts using gradient projection and flash-exposure sampling. In *Proc. ACM SIGGRAPH*, pages 828–835, July 2005.

[2] K. Gai, Z. Shi, and C. Zhang. Blindly separating mixtures of multiple layers with spatial shifts. In *Proc. IEEE CVPR*, pages 1–8, June 2008.

[3] K. Gai, Z. Shi, and C. Zhang. Blind separation of superimposed moving images using image statistics. *IEEE Trans. Pattern Anal. Mach. Intell.*, 34(1):19–32, Jan. 2012.

[4] Y. Hu, D. Zhang, J. Ye, X. Li, and X. He. Fast and accurate matrix completion via truncated nuclear norm regularization. *IEEE Trans. Pattern Anal. Mach. Intell.*, 35(9):2117–2130, Sept. 2013.

[5] J. H. Kim, J. Y. Sim, and C. S. Kim. Video deraining and desnowing using temporal correlation and low-rank matrix completion. *IEEE Trans. Image Process.*, 24(9):2658–2670, Sept. 2015.

[6] N. Kong, Y. W. Tai, and J. S. Shin. A physically-based approach to reflection separation: From physical modeling to constrained optimization. *IEEE Trans. Pattern Anal. Mach. Intell.*, 36(2):209–221, Feb. 2014.

[7] J. Kopf, F. Langguth, D. Scharstein, R. Szeliski, and M. Goesele. Image-based rendering in the gradient domain. *ACM Trans. Graph.*, 32(6), Nov. 2013.

[8] A. Levin and Y. Weiss. User assisted separation of reflections from a single image using a sparsity prior. *IEEE Trans. Image Process.*, 29(9):1647–1654, Sept. 2007.

[9] J. Li, L. Luo, F. Zhang, J. Yang, and D. Rajan. Double low rank matrix recovery for saliency fusion. *IEEE Trans. Image Process.*, 25(9):4421–4432, Sept. 2016.

[10] Y. Li and M. S. Brown. Exploiting reflection change for automatic reflection removal. In *Proc. IEEE ICCV*, pages 2432–2439, Dec. 2013.

[11] Y. Li and M. S. Brown. Single image layer separation using relative smoothness. In *Proc. IEEE CVPR*, pages 2752–2759, June 2014.

[12] C. Liu, J. Yuen, and A. Torralba. Sift flow: Dense correspondence across scenes and its applications. *IEEE Trans. Pattern Anal. Mach. Intell.*, 33(5):978–994, May 2011.

[13] Y. Y. Schechner, N. Kiryati, and J. Shamir. Blind recovery of transparent and semireflected scenes. In *Proc. IEEE CVPR*, pages 38–43, June 2000.

[14] Y. Y. Schechner and J. Shamir. Polarization and statistical analysis of scenes containing a semireflector. *J. Opt. Soc.*, 17(2), Feb. 2000.

[15] Y. Shih, D. Krishnan, F. Durand, and W. T. Freeman. Reflection removal using ghosting cues. In *Proc. IEEE CVPR*, pages 3193–3201, June 2015.

[16] T. Simchony, R. Chellappa, and M. Shao. Direct analytical methods for solving poisson equations in computer vision problems. *IEEE Trans. Pattern Anal. Mach. Intell.*, 12(5):435–446, May 1990.

[17] C. Simon and I. K. Park. Reflection removal for in-vehicle black box videos. In *Proc. IEEE CVPR*, pages 4231–4239, June 2015.

[18] S. N. Sinha, J. Kopf, M. Goesele, D. Scharstein, and R. Szeliski. Image-based rendering for scenes with reflections. *ACM Trans. Graph.*, 31(4):100:1–100:10, July 2012.

[19] N. Srebro and T. Jaakkola. Weighted low-rank approximations. In *Proc. ICML*, pages 720–727, Aug. 2003.

[20] T. Xue, M. Rubinstein, C. Liu, and W. T. Freeman. A computational approach for obstruction-free photography. *ACM Trans. Graph.*, 34(4):79:1–79:11, July 2015.

[21] T. Zhang, B. Ghanem, S. Liu, C. Xu, and N. Ahuja. Low-rank sparse coding for image classification. In *Proc. IEEE ICCV*, pages 281–288, Dec. 2013.